Available online at www.sciencedirect.com
ScienceDirect
Cement & Concrete Composites 29 (2007) 203–217
Cement & Concrete Composites
www.elsevier.com/locate/cemconcomp

Efficacy of CFRP-based techniques for the flexural and shear strengthening of concrete beams

J.A.O. Barros *, S.J.E. Dias, J.L.T. Lima

Department of Civil Engineering, School of Engineering, University of Minho, Azurém, 4800-058 Guimarães, Portugal

Received 9 January 2006; received in revised form 9 September 2006; accepted 11 September 2006
Available online 6 December 2006

Abstract

Near surface mounted (NSM) and externally bonded reinforcement (EBR) strengthening techniques are based on the use of carbon fiber reinforced polymer (CFRP) materials and have been used for the structural rehabilitation of concrete structures. In the present work, the efficacies of the NSM and EBR techniques for the flexural and shear strengthening of reinforced concrete beams are compared carrying out two experimental groups of tests. For the flexural strengthening, the efficacy of applying CFRP laminates according to NSM is compared to those resulting from applying CFRP laminates and wet lay-up CFRP sheets according to EBR technique. The influences of the equivalent reinforcement ratio (steel and laminates) and spacing of the laminates on the efficiency of the NSM technique for the flexural strengthening is also investigated. A numerical strategy is implemented to analyze the applicability of the FRP effective strain concept, proposed by ACI and *fib* in the design of FRP systems for the flexural strengthening. To assess the efficacy of the NSM technique for the shear strengthening of concrete beams, four beam series of distinct depth and longitudinal tensile steel reinforcement ratio are tested. Each series is composed of one beam without any shear reinforcement and one beam using the following shear reinforcing systems: conventional steel stirrups; strips of wet lay-up CFRP sheet of U configuration applied according to EBR technique; and laminates of CFRP embedded into vertical or inclined (45°) pre-cut slits on the concrete cover of the beam lateral faces, according to the NSM technique. Using the obtained experimental results, the performance of the analytical formulations proposed by ACI, *fib* and Italian guidelines is appraised.

Keywords: CFRP; Flexural strengthening; Shear strengthening; Reinforced concrete beams; EBR; NSM

1. Introduction

Near surface mounted (NSM) is one of the most recent and promising strengthening techniques for reinforced concrete (RC) structures. NSM is based on the use of circular [1] or rectangular cross section bars [2] of carbon or glass fiber reinforced polymer (CFRP or GFRP) materials installed into pre-cut slits opened on the concrete cover of the elements to strengthen. NSM requires no surface preparation work and, after cutting the slit, requires minimal installation time compared to the externally bonded reinforcing (EBR) technique. A further advantage associated with NSM is its ability to significantly reduce the probability of harm resulting from acts of vandalism, mechanical damages and aging effects. When NSM is used, the appearance of a structural element is practically unaffected by the strengthening intervention. Since both faces of the laminate are bonded to concrete when using CFRP laminates, high strengthening efficacy has been pointed to the NSM technique on the flexural [3–7] and shear strengthening [8,9] of concrete structures.

In the present work the effectiveness of the NSM and EBR techniques for the flexural and shear strengthening of reinforced concrete beams is compared. For this purpose, two groups of four point beam bending experimental tests were carried out, one for the flexural and the other for the shear strengthening.

* Corresponding author. Tel.: +35 1253510210; fax: +35 1253510217.
E-mail address: barros@civil.uminho.pt (J.A.O. Barros).

0958-9465/$ - see front matter © 2006 Elsevier Ltd. All rights reserved.
doi:10.1016/j.cemconcomp.2006.09.001

For the flexural strengthening, the influence of the longitudinal equivalent reinforcement ratio, $\rho_{l,eq}$, on the strengthening effectiveness of both techniques is assessed. For the NSM technique the influence of the distance between two adjacent slits, a_f, is also analyzed. To assess the applicability of the effective strain concept proposed by ACI [10] and *fib* [11] on the design of flexural strengthening systems, a numerical strategy was used, performing back-fitting analysis supported on the force–deflection relationship obtained in the flexural experimental program carried out in the present research program. The numerical results were also used to propose a new approach for the evaluation of the effective strain in the context of the NSM flexural strengthening design.

For the shear strengthening, the influences of the longitudinal steel reinforcement ratio, ρ_{sl}, and the beam depth on the strengthening effectiveness of both NSM and EBR techniques are evaluated. In the shear strengthening program, the influence of the inclination of the CFRP laminates in the NSM technique is also investigated. The recent Italian Standard for FRP structural strengthening [12] includes an analytical formulation for the design of EBR shear strengthening FRP systems for concrete beams. The performance of this analytical formulation is assessed and compared to the one obtained when using ACI and *fib* proposals.

2. Strengthening techniques

The NSM technique was made up of the following steps: (1) using a diamond blade cutter, slits of 4–5 mm width and 12–15 mm depth were cut on the concrete surface of the elements to strengthen; (2) slits were cleaned by compressed air; (3) CFRP laminates were cleaned by acetone; (4) epoxy adhesive was produced according to supplier recommendations; (5) slits were filled with the epoxy adhesive; (6) epoxy adhesive was applied on the faces of the laminates; and (7) laminates were introduced into the slits and epoxy adhesive in excess was removed.

To apply the wet lay-up strips of CFRP sheet by EBR technique, the following procedures were executed: (1) on the zones of the beams surfaces where the strips of sheet would be glued, an emery was applied to remove the superficial cement paste (in the shear strengthening experimental program the beam's edges were also rounded); (2) the residues were removed by compressed air; (3) a layer of primer was applied to regularize the concrete surface and to enhance the adherence capacity of the concrete substrate; and (4) using epoxy resin, the strips of sheet were glued on the faces of the beam. In cases that laminates were applied according to EBR technique, identical procedures to the ones adopted in EBR sheets were followed, but instead of epoxy resin it was used adhesive epoxy to bond the laminates to concrete.

3. Materials

3.1. Concrete and steel bars

Table 1 includes the values of the main properties of the concrete and steel bars used in the experimental program. The average values of the concrete compressive strength at 28 days (f_{cm}) and at the date of testing the beams ($f_{cm,j}$) were evaluated from uniaxial compression tests (three for each series, at least) with cylinders of 150 mm diameter and 300 mm height. Steel bars were tested according to the recommendations of the European standard EN 10 002-1 [13] and each result is the average of at least three tests.

3.2. CFRP systems

Two CFRP systems were used in the present work: unidirectional wet lay-up sheets (80 mm width in the flexural strengthening and 25 mm width in the shear strengthening) and precured laminates ($1.4 \times 9.6\ mm^2$ cross sectional area in the flexural strengthening and $1.4 \times 10\ mm^2$ cross sectional area in the shear strengthening). The values of the properties of the CFRP systems are indicated in Table 2. For the laminates, six tests were also carried out according to the ISO 527-5 recommendations [14].

Table 1
Properties of the concrete and steel bars

Element type	Concrete		Steel		
	f_{cm} (MPa)	$f_{cm,j}$ (MPa)	ϕ_s (mm)	f_{sym} (MPa)	f_{sum} (MPa)
Flexural strengthening program	44.2	52.2 (70 days)	5	788	890
			6.5	627	765
Shear strengthening program	37.6[a]	49.2[a] (227 days)	6 (stirrups)	540	694
			6 (long.)	622[a]	702[a]
				618[b]	691[b]
	49.5[b]	56.2[b] (105 days)	10	464	581
			12	574[a]	672[a]
				571[b]	673[b]

[a] A series.
[b] B series.

Table 2
Properties of the CFRP materials

CFRP system				Main properties			
Type		Material		Tensile strength (MPa)	Young's modulus (GPa)	Ultimate strain (%)	Thickness (mm)
S&P C-Sheet (wet lay-up sheet)	Sheet	Primer[a]		12	0.7	3.0	–
		Epoxy[a]		54	3.0	2.5	–
		Flexural strengthening prog.	C-Sheet 240[a]	3700	240.0	1.5	0.111
		Shear strengthening prog.	C-Sheet 530[a]	3000	390.0	0.8	0.167
CFK 150/2000 (precured laminate)	Laminate	Adhesive[a]		16–22	5.0	–	–
		Flexural strengthening prog.[b]		2740	158.8	1.7	1.4
		Shear strengthening prog.[b]		2286	166.0	1.3	1.4

[a] According to the supplier.
[b] Evaluated from experimental tests.

4. Flexural strengthening

4.1. Experimental program

4.1.1. Geometry, reinforcement arrangements, loading and supporting conditions of the beams

Fig. 1 represents the geometry of the beam type of the experimental program, the distinct reinforcement arrangements and the number and position of the CFRP strengthening systems of the different cross sections of the tested beams. The experimental program was composed by 24 beams, with two beams for each reinforcement configuration. The load configuration and the support conditions are also schematized. The cross sectional area of the CFRP systems was evaluated in order to impose a similar $A_f E_f / A_{sl} E_s$ ratio within the beams of the experimental program, where A_f and E_f are the CFRP cross sectional area and the Young's Modulus of the CFRP systems, and A_{sl} and E_s (200 GPa) are the cross sectional area and the Young's Modulus of the longitudinal tensile steel bars. Shear reinforcement was selected to assure bending failure prior to shear failure for all beams. The beams were tested at the age of about 70 days. A closed-loop servo-controlled equipment was used, and the force applied by the servo-actuator of 500 kN capacity was controlled by the displacement registered in the LVDT placed at beam midspan, imposing a displacement ratio of 20 μm/s.

4.1.2. Results

The force–deflection relationships for the series of tested beams are depicted in Fig. 2. Each curve represents the average of the two tested beams. The strengthening efficacy

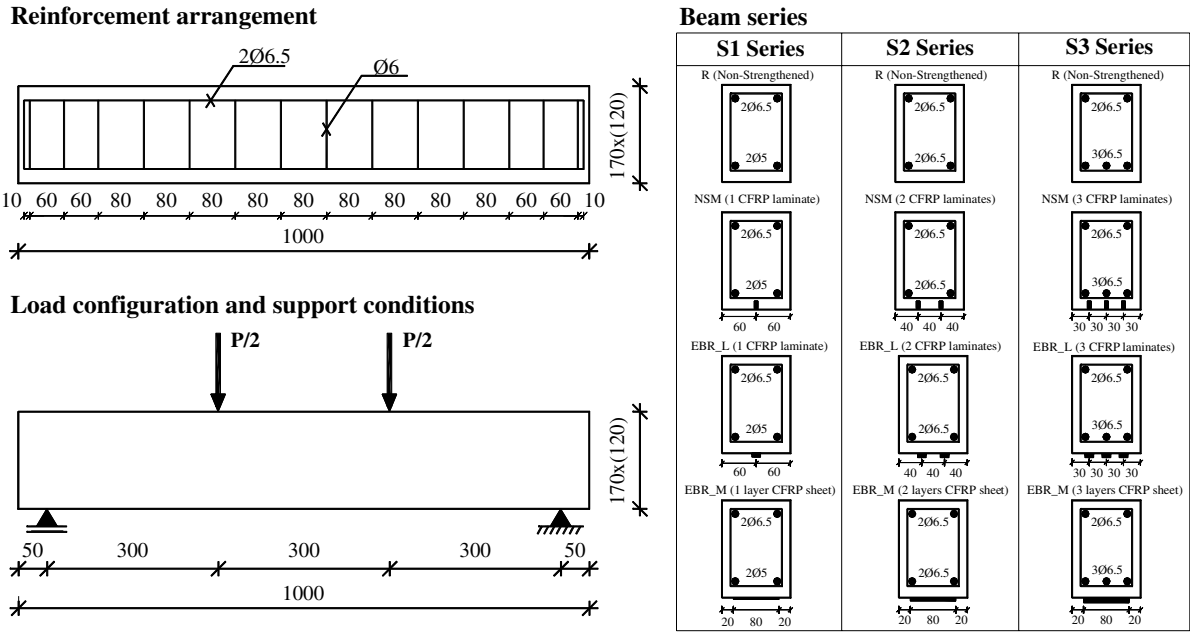

Fig. 1. Beam series for the flexural strengthening (dimensions in mm).

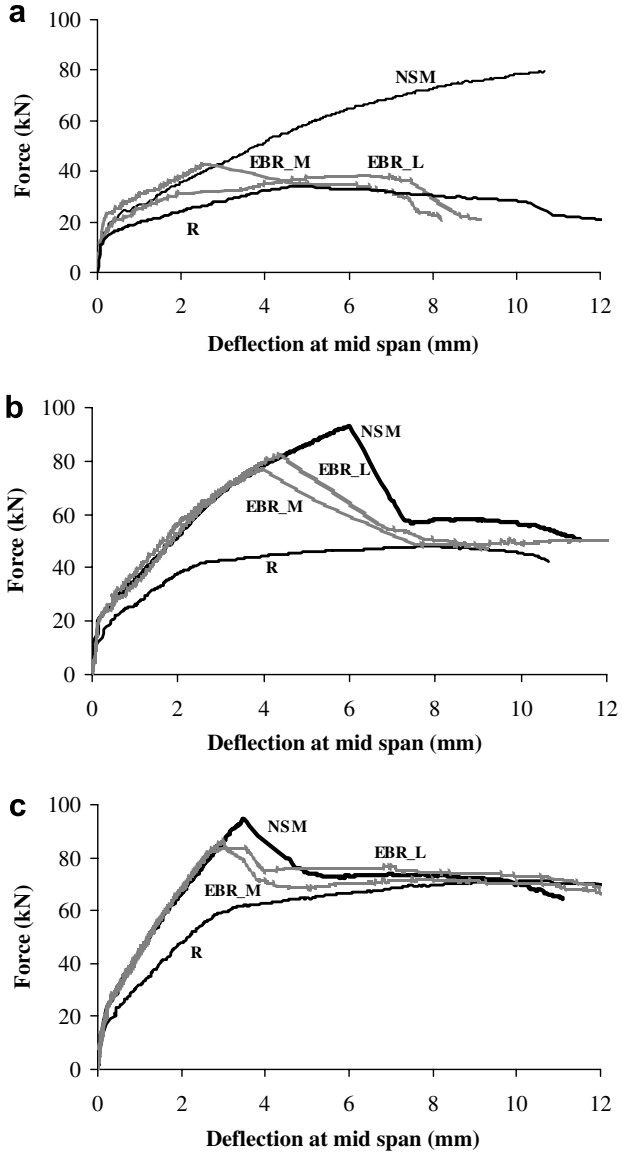

Fig. 2. Force–deflection relationships of the flexural strengthening beams series: (a) S1; (b) S2; (c) S3.

is evaluated in terms of the service (P_{serv}) and the maximum (P_{max}) load (see Table 3). P_{serv} is the load for a deflection of $L/400 = 2.25$ mm, where L is the beam span. $P_{serv}(S)$ and $P_{max}(S)$ are the service and maximum load of a strengthened beam, respectively, while $P_{serv}(R)$ and $P_{max}(R)$ are the service and maximum load of the reference beam. In

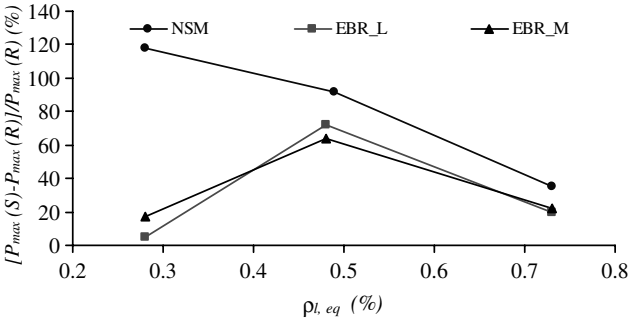

Fig. 3. Strengthening efficacy *vs* longitudinal equivalent reinforcement ratio.

Table 3 the equivalent reinforcement ratio, $\rho_{l,eq} = A_{sl}/(bd_s) + (A_f E_f/E_s)/(bd_f)$, is also indicated, where b is the beam width and d_s and d_f are the effective depth of the longitudinal steel bars and CFRP systems, respectively. The influence of the $\rho_{l,eq}$ on the strengthening efficacy index is graphically represented in Fig. 3. In terms of the beam load carrying capacity, the NSM technique was the most effective one. The effectiveness, however, decreased with the increase of $\rho_{l,eq}$. In terms of service load, the EBR based on the use of wet lay-up CFRP sheets was the most efficient, since E_f and d_f were the largest ones.

The typical failures modes are indicated in Table 4 and photos of these representative failure modes are shown in Fig. 4.

4.2. Appraisal of the ACI and fib analytical formulations

The load carrying capacity of EBR strengthened RC beams can be estimated from the design resisting bending moment of the cross section of these beams. ACI [10] and *fib* [11] analytical formulations propose the following equations:

$$M_{Rd} = A_{sl} f_{syd}(d_s - 0.4x) + \gamma_f A_f f_{fe}(h - 0.4x) \quad \text{ACI} \qquad (1)$$

$$M_{Rd} = A_{sl} f_{syd}(d_s - 0.4x) + A_f f_{fe}(h - 0.4x) \quad \textit{fib} \qquad (2)$$

where h is the height of the beam cross section, x is the position of the neutral axis, f_{fe} is the effective tensile stress at ultimate conditions in the FRP ($f_{fe} = E_f \varepsilon_{fe}$), and $\gamma_f = 0.85$ is a safety factor. The meaning of the other variables was already presented. In Eqs. (1) and (2) it was assumed that the thickness of the CFRP laminates and sheets, as well as the corresponding adhesive materials

Table 3
Main results of the flexural strengthening beam series

Beam designation	$\rho_{l,eq}$ (%) Series			P_{ser} (kN) Series			$\frac{P_{ser}(S)-P_{ser}(R)}{P_{ser}(R)}$ (%) Series			P_{max} (kN) Series			$\frac{P_{max}(S)-P_{max}(R)}{P_{max}(R)}$ (%) Series		
	S1	S2	S3	S1	S2	S3	S1	S2	S3	S1	S2	S3	S1	S2	S3
R	–	–	–	22.1	40.5	51.5	–	–	–	36.6	48.5	71.8	–	–	–
NSM	0.28	0.49	0.73	37.5	56.3	71.5	70	39	39	79.9	93.3	96.6	118	92	35
EBR_L	0.28	0.48	0.73	31.9	57.6	74.1	44	42	44	38.6	83.5	86.5	5	72	20
EBR_M	0.28	0.48	0.73	40.3	59.5	73.4	82	47	43	43.0	79.5	87.3	17	64	22

Table 4
Typical failure modes

Strengthening system		Failure mode description
Without CFRP		The longitudinal steel yielded and the concrete crushed in the most compressed zone
NSM		Yielding of the longitudinal steel reinforcement and delamination of the concrete cover
EBR laminates	1 or 2 laminates	Debonding of the laminate(s) at the concrete/laminate interface
	3 laminates	Yielding of the longitudinal steel and debonding of the laminates at the concrete/laminate interface (one beam) Yielding of the longitudinal steel and delamination of the concrete cover (one beam)
EBR sheets	1 layer	Rupture of the CFRP sheet in the beam failure cross section
	2 layers	Yielding of the longitudinal steel and rupture of the CFRP sheet in the beam failure cross section
	3 layers	Yielding of the longitudinal steel and delamination of the concrete cover

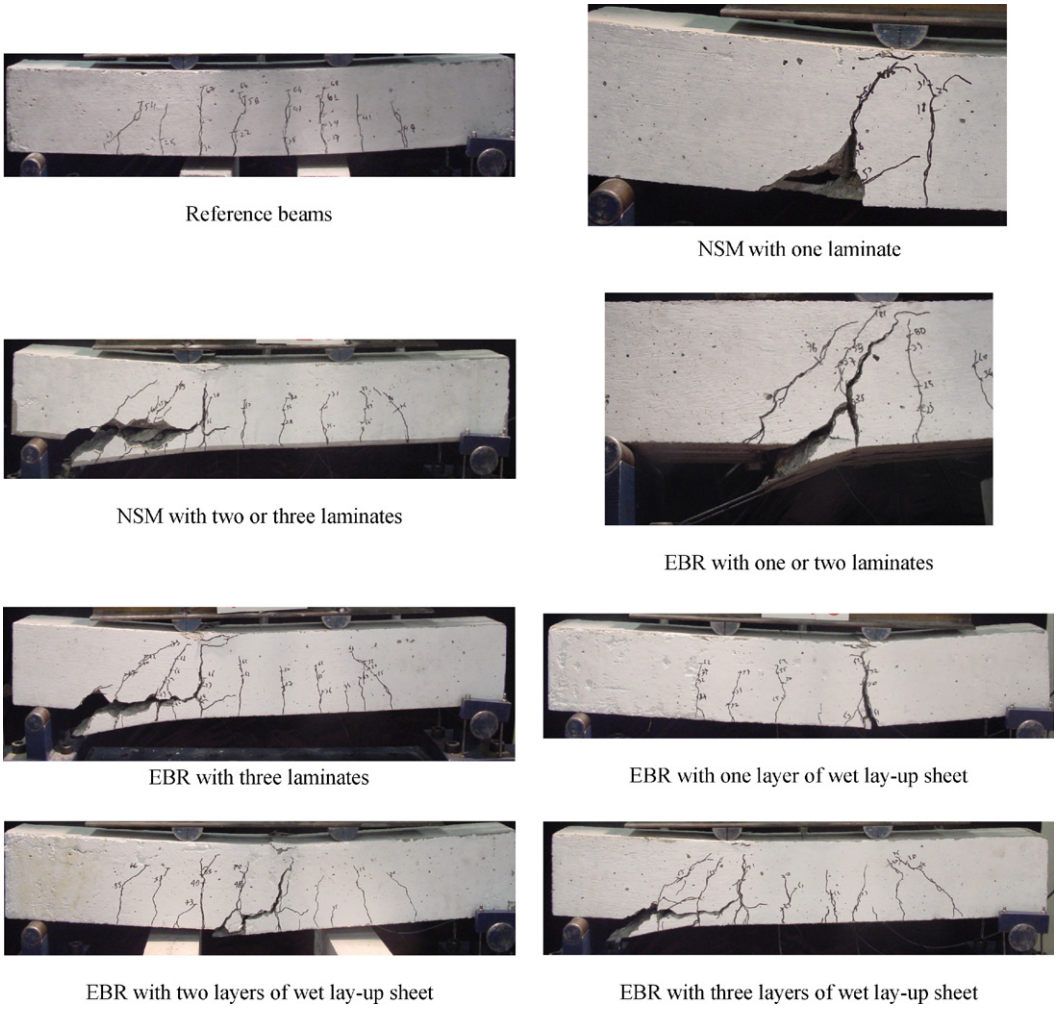

Fig. 4. Photos of the typical failure modes.

can be neglected for the evaluation of internal arm of the FRP system.

In the ACI approach, the effective strain in the FRP material, ε_{fe}, is evaluated from the following equation:

$$\varepsilon_{fe} = \varepsilon_{cu}\left(\frac{h-x}{x}\right) - \varepsilon_{ci} \leqslant k_m \varepsilon_{fu} \tag{3}$$

where ε_{cu} is the maximum acceptable concrete compressive strain (=0.003), ε_{ci} is the initial strain of the concrete substrate, ε_{fu} is the FRP design rupture strain and k_m is bond-dependent coefficient that can be obtained from the following equations:

$$k_m = \begin{cases} \frac{1}{60\varepsilon_{fu}}\left(1 - \frac{nE_f t_f}{360\,000}\right) \leqslant 0.90 & \text{for } nE_f t_f \leqslant 180\,000 \\ \frac{1}{60\varepsilon_{fu}}\left(\frac{90\,000}{nE_f t_f}\right) \leqslant 0.90 & \text{for } nE_f t_f > 180\,000 \end{cases} \tag{4}$$

where n is the number of plies of FRP flexural reinforcement at the cross section of the member where the resisting

bending moment is being computed, and t_f is the thickness of the FRP material.

In the *fib* approach the effective strain may be calculated according to the following equation:

$$\varepsilon_{fe} = \alpha c_1 k_c k_b \sqrt{\frac{f_{ctm}}{nE_f t_f}} \quad (5)$$

where α is a reduction factor, equal to 0.9, to account for the influence of inclined cracks on the bond strength ($\alpha = 1$ in beams with sufficient internal and external shear reinforcement and in slabs), c_1 is an empirical factor assumed to be 0.64 for CFRP, k_c is a factor accounting for the state of concrete compaction ($k_c = 1.0$, but for CFRP bonded to concrete faces with low compaction, e.g. faces not in contact with the formwork during casting, $k_c = 0.67$) and k_b is a geometry factor:

$$k_b = 1.06\sqrt{\left(2 - \frac{b_f}{b}\right) \Big/ \left(1 + \frac{b_f}{400}\right)} \geqslant 1.0 \quad (6)$$

where b_f is the width of the FRP system and b the width of the beam cross section. Table 5 includes the values of the parameters used in the analytical simulations. When the design values of these parameters are used, the values of the beam maximum load carrying capacity, P_{max}^{ana}, estimated by ACI and *fib* formulations are compared to the experimental ones in Table 6, while Table 7 includes the values obtained from the same exercise, but using the average values for the material properties (all safety factors were

Table 5
Values of the concrete, steel and CFRP properties for the analytical and numerical simulation

Materials	Average values (experimental values)		Design values	
			ACI formulation	*fib* formulation
Concrete		$f_{cm} = 52.2$ MPa	$f'_c = 42.9$ MPa[a]	$f_{cd} = 44.2$ MPa[b]
Steel	$\phi 5$	$f_{sym} = 788$ MPa	$f_{syd} = f_y = 685.2$ MPa[c]	$f_{syd} = 685.2$ MPa[c]
	$\phi 6.5$	$f_{sym} = 627$ MPa	$f_{syd} = f_y = 545.2$ MPa[c]	$f_{syd} = 545.2$ MPa[c]
CFRP laminate		$E_f = 150$ GPa; $\varepsilon_f = 17‰$	$E_f = 150$ GPa; $\varepsilon_f = 14‰$[d]	
CFRP sheet		–	$E_f = 240$ GPa; $\varepsilon_f = 15‰$[d]	

[a] $f'_c = (f_{cm} - 5)/1.1$ [25].
[b] $f_{cd} = (f_{cm} - 8)/1.5$ [20].
[c] $f_{syd} = f_{sym}/1.15$.
[d] According to the supplier.

Table 6
Experimental versus analytical values, using design values for the material properties (EBR)

Beam designation		Experimental		ACI formulation				*fib* formulation			
		P_{max}^{exp} (kN)	M_{max}^{exp} (kN m)	ε_{fe} (‰)	M_{max}^{ana} (kN m)[a]	P_{max}^{ana} (kN)	$P_{max}^{exp}/P_{max}^{ana}$	ε_{fe} (‰)	M_{max}^{ana} (kN m)	P_{max}^{ana} (kN)	$P_{max}^{exp}/P_{max}^{ana}$
S1 series	EBR_L	38.6	5.79	7.14	5.24	35.0	1.10	3.93	5.07	33.8	1.14
	EBR_M	43.0	6.45	13.50	6.98	46.6	0.92	8.48	6.67	44.4	0.97
S2 series	EBR_L	83.5	12.53	7.14	8.09	54.0	1.55	3.80	7.45	49.6	1.68
	EBR_M	79.5	11.93	13.50	11.42	76.1	1.04	6.00	9.0	60.0	1.33
S3 series	EBR_L	86.5	12.98	7.14	11.84	78.9	1.10	3.67	10.73	71.5	1.21
	EBR_M	87.3	13.10	11.19	14.95	99.7	0.88	4.90	12.03	80.2	1.09

[a] The value obtained using Eq. (1) was multiplied by the $\phi(= 0.9)$ strength-reduction factor to attend the ductility level of the cross section [10].

Table 7
Experimental versus analytical values, using average values for the material properties (EBR)

Beam designation		Experimental		ACI formulation				*fib* formulation			
		P_{max}^{exp} (kN)	M_{max}^{exp} (kN m)	ε_{fe} (‰)	M_{max}^{ana} (kN m)	P_{max}^{ana} (kN)	$P_{max}^{exp}/P_{max}^{ana}$	ε_{fe} (‰)	M_{max}^{ana} (kN m)	P_{max}^{ana} (kN)	$P_{max}^{exp}/P_{max}^{ana}$
S1 series	EBR_L	38.6	5.79	6.75	6.80	45.4	0.85	3.82	5.78	38.5	1.00
	EBR_M	43.0	6.45	13.5	9.12	60.8	0.71	8.48	7.40	49.3	0.87
S2 series	EBR_L	83.5	12.53	6.75	10.58	70.5	1.18	3.69	8.49	56.6	1.48
	EBR_M	79.5	11.93	13.5	15.07	100.5	0.79	6.00	10.06	67.1	1.18
S3 series	EBR_L	86.5	12.98	6.75	15.57	103.8	0.83	3.57	12.42	82.8	1.04
	EBR_M	87.3	13.10	12.97	21.52	143.5	0.61	4.90	13.74	91.6	0.95

considered as unitary values). From the analysis of the values included in these two tables it can be concluded that, even when using design values for the material parameters, both ACI and *fib* formulations provide unsafe results for some EBR strengthening arrangements, mainly ACI for the EBR_M strengthening configuration. Independently of using design or average values for the material parameters, *fib* formulation provides larger $P_{max}^{exp}/P_{max}^{ana}$ values than ACI approach.

For the NSM technique, both ACI and *fib* are not yet recommending a strategy to evaluate the FRP effective strain. The analysis of the available research indicates that $\varepsilon_{fe}/\varepsilon_{fu}$ decreases with the increase of $\rho_{l,eq}$, with the decrease of the distance between FRP elements, a_f, and, in case of RC beams, with the decrease of the distance of the FRP elements to the edges of the beam [15]. The concrete resistance, the geometry of the slit, the thickness of the adhesive layers and the properties of the adhesive materials should also have some influence on the value of the $\varepsilon_{fe}/\varepsilon_{fu}$ ratio, however, insufficient research results are available to perform a quantitative estimate of the influence of these last variables on the variation of the $\varepsilon_{fe}/\varepsilon_{fu}$ ratio. The influence of the $\rho_{l,eq}$ on the variation of the $\varepsilon_{fe}/\varepsilon_{fu}$ ratio is represented in Fig. 5, from which a clear tendency for the decrease of $\varepsilon_{fe}/\varepsilon_{fu}$ with the increase of $\rho_{l,eq}$ can be recognized, represented by the following equation:

$$\frac{\varepsilon_{fe}}{\varepsilon_{fu}} = -32.648 \cdot \rho_{l,eq} + 0.9606 \tag{7}$$

The collected values refer to RC beams [4,16,17] and slabs [6,7,18] that failed in bending. If the linear relationship between $\varepsilon_{fe}/\varepsilon_{fu}$ and $\rho_{l,eq}$, indicated in this figure, is used to estimate ε_{fe}, the ACI and *fib* analytical formulations (Eqs. (1) and (2)) lead to the values indicated in Tables 8 and 9 (if design and average values are used for the materials properties, respectively). The analysis of the values of theses tables indicates that, the decrease of the $P_{max}^{exp}/P_{max}^{ana}$ with the increase of the $\rho_{l,eq}$ was much more pronounced from S1 to S3 tested series than was in the experimental

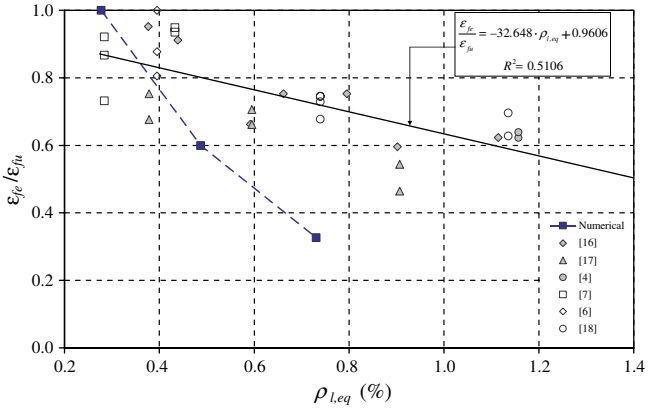

Fig. 5. Strengthening efficacy index *vs* longitudinal equivalent reinforcement ratio for the NSM.

Table 8
Experimental *vs* analytical values, using design values for the material properties (NSM)

Beam designation		Experimental		ACI formulation				*fib* formulation			
		P_{max}^{exp} (kN)	M_{max}^{exp} (kN m)	ε_{fe} (‰)	M_{max}^{ana} (kN m)	P_{max}^{ana} (kN)	$P_{max}^{exp}/P_{max}^{ana}$	ε_{fe} (‰)	M_{max}^{ana} (kN m)	P_{max}^{ana} (kN)	$P_{max}^{exp}/P_{max}^{ana}$
S1 series	NSM	79.9	11.99	12.19	6.38	42.6	1.88	12.19	7.54	50.3	1.59
S2 series	NSM	93.3	14.00	11.25	9.85	65.7	1.42	11.25	11.66	77.8	1.20
S3 series	NSM	96.6	14.49	10.15	13.62	90.8	1.06	8.50	14.55	97.0	1.00

Table 9
Experimental versus analytical values, using average values for the material properties (NSM)

Beam designation		Experimental		ACI and *fib* formulations			
		P_{max}^{exp} (kN)	M_{max}^{exp} (kN m)	ε_{fe} (‰)	M_{max}^{ana} (kN m)	P_{max}^{ana} (kN)	$P_{max}^{exp}/P_{max}^{ana}$
S1 series	NSM	79.9	11.99	14.79 [17.00]	9.41	62.8	1.27 [1.18]
S2 series	NSM	93.3	14.00	13.63 [10.19]	14.88	99.2	0.94 [1.10]
S3 series	NSM	96.6	14.49	12.28 [5.55]	20.50	136.7	0.71 [1.02]

programs of the data included in Fig. 5. The main reason is related to the a_f values that are lower in S3 series than in the major part of the series indicated in Fig. 5. Fig. 6 shows a clear tendency of the increase of the $\varepsilon_{fe}/\varepsilon_{fu}$ with the a_f/b ratio for some of the available NSM flexural strengthened RC beams [4,16,17].

4.3. Numerical simulation

Previous works [3,19] shown that, using a cross section layered model that takes into account the constitutive laws of the intervening materials, and the kinematic and the equilibrium conditions, the deformational behavior of structural elements failing in bending can be predicted from the moment–curvature relation, M–χ, of the representative cross sections of these elements, using the algorithm described elsewhere [3]. To evaluate the M–χ relationship, the beam cross section was discretized in layers of 1 mm thickness. The beam was discretized in 60 Euler–Bernoulli beam elements of two nodes per element. The tangential stiffness matrix of the beam was obtained by assembling the tangential stiffness matrix of these elements. The updated flexural rigidity taking part in the tangential stiffness matrix of each element was obtained from the M–χ relationship corresponding to the cross section of this element. To simulate the concrete compression behavior, the stress–strain relationship recommended by model code CEB-FIP 1993 was used [3,20]. Up to the concrete tensile strength, f_{ct}, the concrete was assumed as behaving linearly. The behavior of the concrete layers in softening and in stiffening [21] was simulated by the trilinear diagram represented in Fig. 7. The data adopted for defining the softening and the stiffening trilinear diagram of the post-cracking behavior of concrete layers, used in the numerical simulation, is indicated in Table 10. The values included in Tables 1 and 2 were used to define the linear parabola and the linear stress–strain diagrams used to model the steel bars and CFRP systems, respectively.

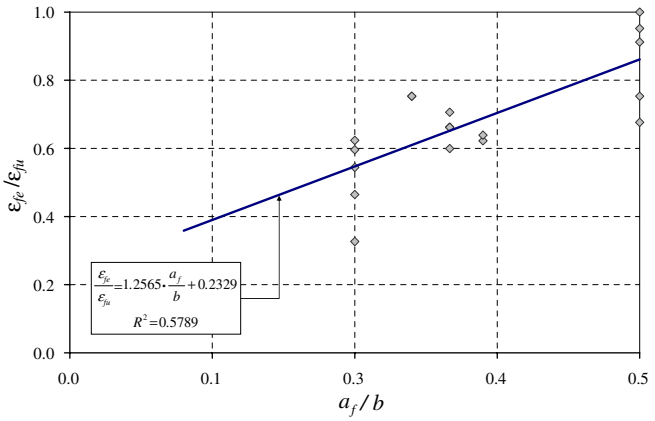

Fig. 6. Influence of the a_f/b ratio on the $\varepsilon_{fe}/\varepsilon_{fu}$.

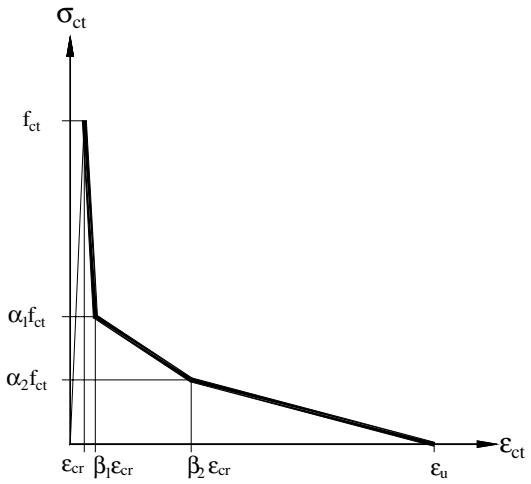

Fig. 7. Trilinear stress–strain diagram for modeling the concrete post-cracking behavior.

The experimental and the numerical force–midspan deflection of each of the beams of S2 series are compared in Fig. 8, from which it can be concluded that the applied numerical strategy is able of fitting, with enough accuracy, the deformational behaviour of the tested beams. Similar accuracy was obtained for the beams of the other two series. The values of the maximum strain in the CFRP systems for the peak load of the tested strengthened beams, obtained from numerical analysis, are compared in Fig. 9, to the effective strain proposed by ACI and *fib* recommendations. From the analysis of this figure, and taking for the basis of comparison the values obtained from the numerical simulation, it is verified that ACI predicts too high $\varepsilon_{fe}/\varepsilon_{fu}$ values for the EBR technique, mainly when using wet lay-up CFRP sheets. For the EBR_M beams, *fib* estimates too high $\varepsilon_{fe}/\varepsilon_{fu}$ values for the lowest value of $\rho_{l,eq}$.

For the NSM technique, Fig. 9 also shows that, when $\rho_{l,eq}$ is greater than of about 0.35%, Eq. (7) predicted higher $\varepsilon_{fe}/\varepsilon_{fu}$ values than the ones obtained from the

Table 10
Values used to define the softening and the stiffening trilinear stress–strain diagram on the numerical simulation

Beam designation		Compression		Tension	Softnening					Stiffening				
		f_{cm} (MPa)	E_c (GPa)	f_{ct} (MPa)	α_1	α_2	β_1	β_2	ε_u (‰)	α_1	α_2	β_1	β_2	ε_u (‰)
S1 series	NSM	52.2	36.1	3.16	0.4	2.0	0.2	10.0	5.19	0.7	10.0	0.3	20	27.2
	EBR_L	52.2	36.1	3.16	0.4	2.0	0.2	10.0	5.19	0.7	10.0	0.3	20	27.2
	EBR_M	52.2	36.1	3.16	0.4	2.0	0.2	10.0	5.19	0.7	10.0	0.3	20	27.2
S2 series	R	52.2	36.1	2.56	0.4	2.0	0.2	10.0	5.19	0.6	5.0	0.4	15	2.5
	NSM	52.2	36.1	3.16	0.4	2.0	0.2	10.0	5.19	0.7	10.0	0.4	15	14.3
	EBR_L	52.2	36.1	3.16	0.4	2.0	0.2	10.0	5.19	0.7	10.0	0.4	15	14.3
	EBR_M	52.2	36.1	3.16	0.4	2.0	0.2	10.0	5.19	0.7	10.0	0.4	15	14.3
S3 series	R	52.2	36.1	2.56	0.4	2.0	0.2	10.0	5.19	0.6	5.0	0.4	15	2.5
	NSM	52.2	36.1	3.16	0.4	2.0	0.2	10.0	5.19	0.7	10.0	0.3	20	2.3
	EBR_L	52.2	36.1	3.16	0.4	2.0	0.2	10.0	5.19	0.7	10.0	0.3	20	2.3
	EBR_M	52.2	36.1	3.16	0.4	2.0	0.2	10.0	5.19	0.7	10.0	0.3	20	2.3

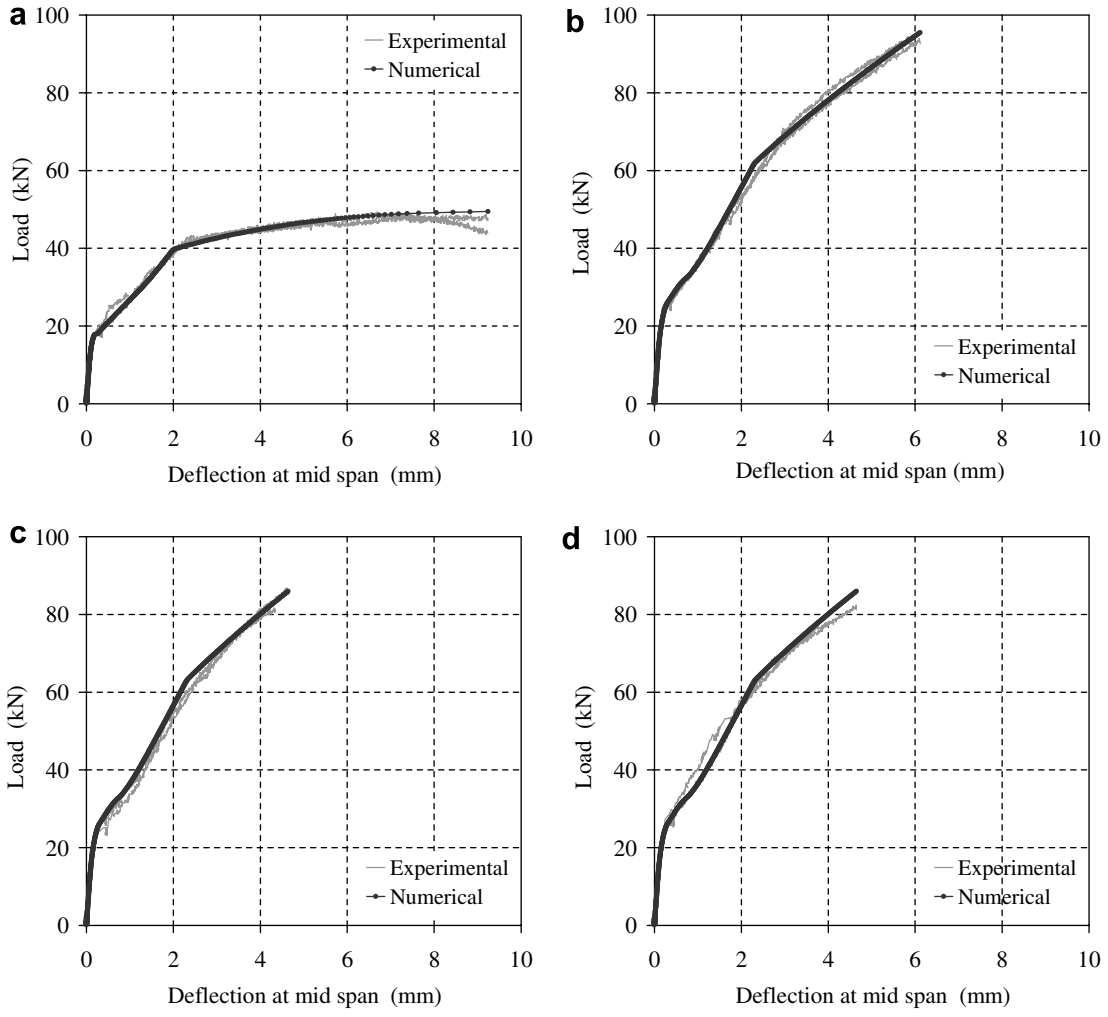

Fig. 8. Experimental *vs* numerical force–deflection curves for the S2 series: (a) reference beam; (b) NSM; (c) EBR_L; (d) EBR_M.

numerical analysis. If ε_{fe} is estimated using the $\varepsilon_{fe}/\varepsilon_{fu}$–$\rho_{l,eq}$ relationship derived from the values obtained in the numerical simulation of the tested NSM beams (dashed line in Fig. 9), the $P_{max}^{exp}/P_{max}^{ana}$ values were much more uniform (see values inside square brackets of Table 9) than those determined from the use of Eq. (7), since the dashed line predicts with higher accuracy the FRP effective strain in the NSM tested beams. The values inside square brackets

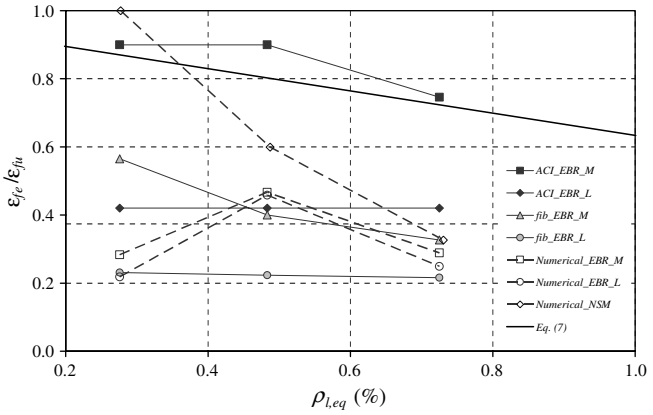

Fig. 9. Experimental *vs* numerical $\varepsilon_{fe}/\varepsilon_{fu}$–$\rho_{l,eq}$ relationship.

of Table 9 were obtained from Eq. (1), which is equal to Eq. (2), since $\gamma_f = 1.0$ when average values for the material properties are used.

5. Shear strengthening

5.1. Experimental program

5.1.1. Geometry, reinforcement arrangements, loading and supporting conditions of the beams

The experimental program was composed by four series of tests. The geometry, reinforcement arrangement and support conditions of the beams of these series are indicated in Fig. 10. Each series was constituted by a beam without any shear reinforcement (R) and a beam for each of the following shear reinforcing systems: steel stirrups (S), strips of CFRP sheet (M), laminate strips of CFRP at 90° with the beam axis (VL), and laminate strips of CFRP at 45° with the beam axis (IL). The shear span, *a*, on the series of beams was two times the depth of the corresponding beams. The concrete clear cover for the top, bottom and lateral faces of the beams was 15 mm. The amount of shear reinforcement applied on the four reinforcing systems was evaluated in order to assure that

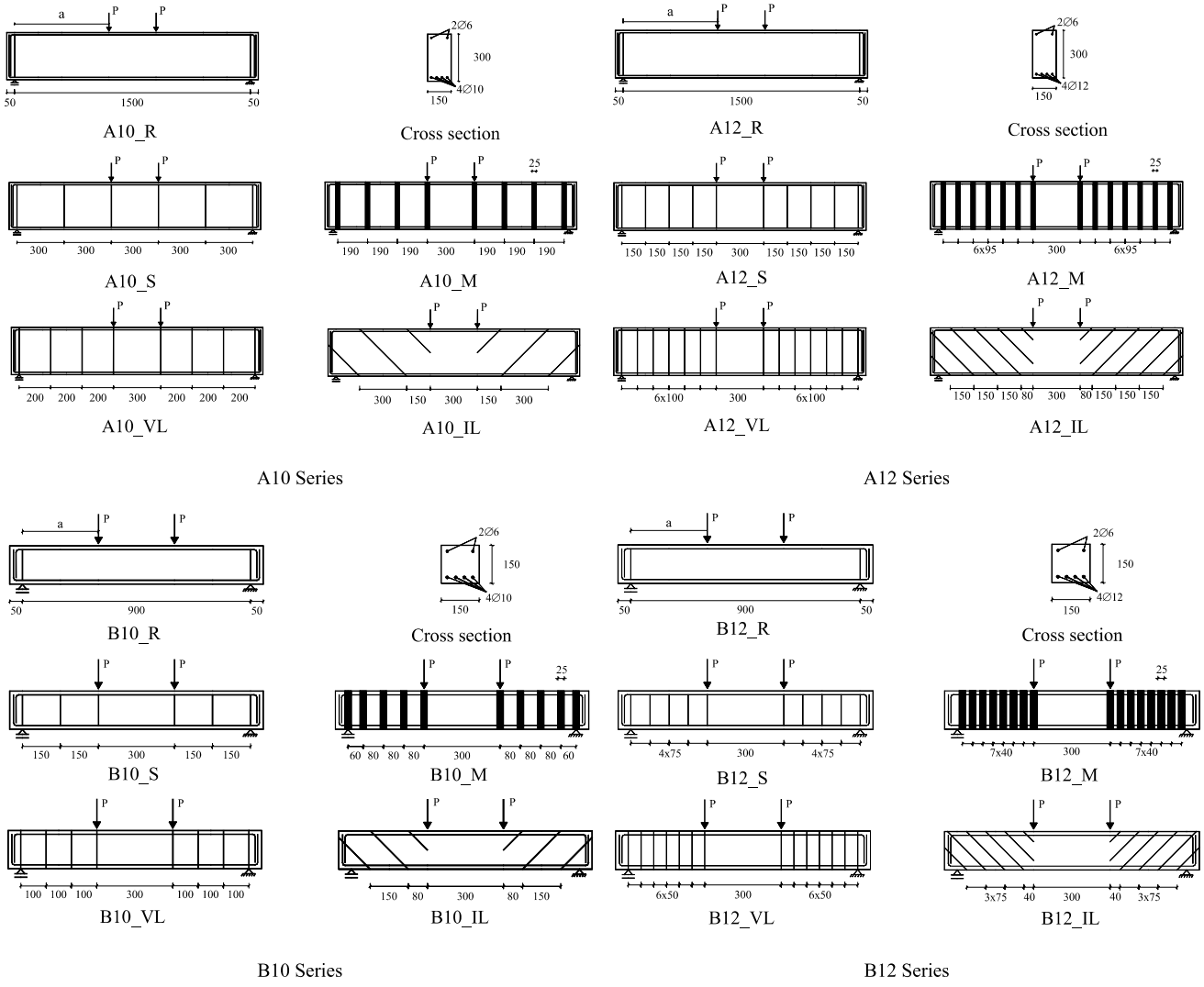

Fig. 10. Beam series for the shear strengthening (dimensions in mm).

Table 11
Beam series for the shear strengthening

Beam designation			Shear strengthening systems			
			Material	Quantity	Spacing (mm)	Angle (°)
A Series	A10 Series	A10_R	–	–	–	–
		A10_S	Steel stirrups	6ϕ6 of two branches	300	90
		A10_M	Strips of S&P C-Sheet 530	8 × 2 layers of 25 mm (U shape)	190	90
		A10_VL	S&P laminates of CFK 150/2000	16 CFRP laminates	200	90
		A10_IL	S&P laminates of CFK 150/2000	12 CFRP laminates	300	45
	A12 Series	A12_R	–	–	–	–
		A12_S	Steel stirrups	10ϕ6 of two branches	150	90
		A12_M	Strips of S&P C-Sheet 530	14 × 2 layers of 25 mm (U shape)	95	90
		A12_VL	S&P laminates of CFK 150/2000	28 CFRP laminates	100	90
		A12_IL	S&P laminates of CFK 150/2000	24 CFRP laminates	150	45
B Series	B10 Series	B10_R	–	–	–	–
		B10_S	Steel stirrups	6ϕ6 of two branches	150	90
		B10_M	Strips of S&P C-Sheet 530	10 × 2 layers of 25 mm (U shape)	80	90
		B10_VL	S&P laminates of CFK 150/2000	16 CFRP laminates	100	90
		B10_IL	S&P laminates of CFK 150/2000	12 CFRP laminates	150	45
	B12 Series	B12_R	–	–	–	–
		B12_S	Steel stirrups	10ϕ6 of two branches	75	90
		B12_M	Strips of S&P C-Sheet 530	16 × 2 layers of 25 mm (U shape)	40	90
		B12_VL	S&P laminates of CFK 150/2000	28 CFRP laminates	50	90
		B12_IL	S&P laminates of CFK 150/2000	24 CFRP laminates	75	45

all beams would fail in shear, at a similar load carrying capacity [10,20]. Table 11 includes general information of the beams composing the four series. Further information can be found elsewhere [8].

5.1.2. Results

The relationship between the force and the deflection at midspan of the tested beams is represented in Fig. 11. Table 12 includes the main results obtained in the four series. Adopting the designation of $F_{\max,K\_R}$ and $F_{\max,K\_S}$ for referring the maximum load of a beam without shear reinforcement and a beam reinforced with steel stirrups, respectively, (K represents the series of tests) the ratios $F_{\max}/F_{\max,K\_R}$ and $F_{\max}/F_{\max,K\_S}$ were determined for assessing the efficacy of the shear strengthening techniques, in terms of increasing the beam load carrying capacity.

The unreinforced shear R beams failed by the formation of one shear failure crack and the longitudinal tensile reinforcement did not yield. In the beams reinforced with steel stirrups (S beams) a shear failure crack occurred. The sudden loss of the load carrying capacity in the S beams corresponds to the moment when a stirrup crossing the shear failure crack ruptured. In general, M beams failed by the formation of a shear crack. In these beams, immediately after the CFRP strips crossing the shear failure crack have peeled-off, the CFRP strips crossing the horizontal path of the shear crack ruptured due to an abrupt increment of tensile and shear stresses in the CFRP, as a result of the crack opening and crack sliding. B12_M beam had a distinct failure mode. This beam failed by the formation of two "concrete lateral walls" that have separated from the interior concrete volume. A shear crack formed in this interior concrete volume, and finally the "lateral walls" ruptured. This complex type of failure also occurred in B10_VL, B10_IL, B12_VL and B12_IL beams. In A10_VL beam, after the longitudinal tensile reinforcement has yielded, a shear failure crack formed and the shorter bond length of the CFRP laminate, crossing this crack, debonded. A12_VL beam failed in shear and the CFRP laminate crossing this crack debonded by its shorter bond length. Finally, A10_IL and A12_IL beams ruptured by the formation of a flexural failure crack.

From the results obtained, the following main conclusions can be pointed out:

- The CFRP shear strengthening systems applied in the present work increased significantly the shear resistance of concrete beams.
- The NSM shear strengthening technique was the most effective of the CFRP systems. This efficacy was not only in terms of the beam load carrying capacity, but also in terms of deformation capacity at beam failure. Using the load carrying capacity of the unreinforced beams for comparison purposes, the beams strengthened by EBR and NSM techniques presented an average increase of 54% and 83%, respectively.
- Increasing the beam depth, laminates at 45° became more effective than vertical laminates.
- $F_{\max}$ of the beams reinforced with steel stirrups and $F_{\max}$ of the beams strengthened by NSM technique were almost similar.
- Failure modes of the beams strengthened by the NSM technique were not as fragile as the ones observed in the beams strengthened by the EBR technique.

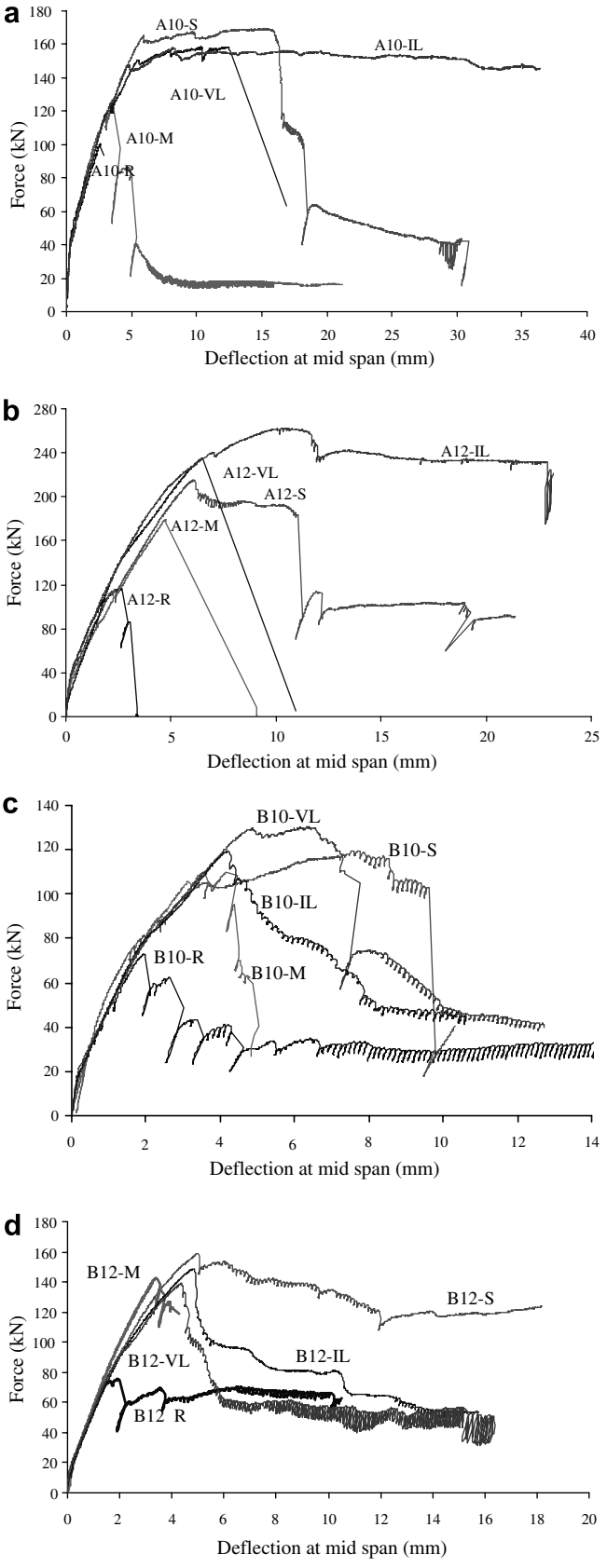

Fig. 11. Force–deflection relationships of the shear strengthening beams: (a) A10 Series; (b) A12 Series; (c) B10 Series; (d) B12 Series.

Table 12
Main results of the shear strengthening beam series

Beam designation	Shear reinforcing system	$F_{\max,K}$ (kN)	$\frac{F_{\max,K}}{F_{\max,K\_R}}$	$\frac{F_{\max,K}}{F_{\max,K\_S}}$
A10_R	–	100.40	1.00	0.59
A10_S	Steel stirrups	169.35	1.69	1.00
A10_M	Strips of sheet	122.06	1.22	0.72
A10_VL	Vertical laminates	158.64	1.58	0.94
A10_IL	Inclined laminates	157.90	1.57	0.93
A12_R	–	116.50	1.00	0.54
A12_S	Steel stirrups	215.04	1.85	1.00
A12_M	Strips of sheet	179.54	1.54	0.83
A12_VL	Vertical laminates	235.11	2.02	1.09
A12_IL	Inclined laminates	262.38	2.25	1.22
B10_R	–	74.02	1.00	0.61
B10_S	Steel stirrups	120.64	1.63	1.00
B10_M	Strips of sheet	111.14	1.50	0.92
B10_VL	Vertical laminates	131.22	1.77	1.09
B10_IL	Inclined laminates	120.44	1.63	1.00
B12_R	–	75.70	1.00	0.48
B12_S	Steel stirrups	159.10	2.10	1.00
B12_M	Strips of sheet	143.00	1.89	0.90
B12_VL	Vertical laminates	139.20	1.84	0.87
B12_IL	Inclined laminates	148.50	1.96	0.93

5.2. Appraisal of the ACI, fib and CNR analytical formulations

In a previous work, the performance of the ACI and *fib* formulations was assessed for the EBR shear strengthening of concrete beams [22]. Therefore, the main purpose of the present section is to assess the applicability of the recent Italian design guideline, CNR, [12,23] for the EBR shear strengthening, and compare its performance with the one of ACI and *fib* formulations.

According to the CNR formulation, the shear capacity carried by the FRP in case of U jacketed reinforcement, can be expressed as

$$V_{\mathrm{fd}} = \frac{1}{\gamma_{\mathrm{Rd}}} \cdot 0.9 \cdot d_{\mathrm{s}} \cdot f_{\mathrm{fe}} \cdot 2 \cdot t_{\mathrm{f}} \cdot (\cot\theta + \cot\beta) \cdot \frac{w_{\mathrm{f}}}{s_{\mathrm{f}}} \tag{8}$$

where γ_{Rd} is a partial safety factor covering the uncertainty of the model, taken equal to 1.2, f_{fe} is the effective design stress of the FRP shear reinforcement, β is the angle formed by the FRP shear reinforcement with the beam axis, θ is the critical shear crack angle, s_{f} and w_{f} are the strip spacing and width, respectively, measured orthogonally to the fiber direction (see Fig. 12).

In (8), the effective design stress of the FRP shear reinforcement, f_{fe}, can be evaluated as

$$f_{\mathrm{fe}} = f_{\mathrm{fdd}} \cdot \left(1 - \frac{1}{3} \cdot \frac{L_{\mathrm{e}} \cdot \sin\beta}{z'}\right), \quad z' = \min\{0.9 \cdot d, h_{\mathrm{w}}\} \tag{9}$$

where L_{e} is the effective bond length defined as

$$L_{\mathrm{e}} = \sqrt{\frac{E_{\mathrm{f}} \cdot t_{\mathrm{f}}}{2 \cdot f_{\mathrm{ctm}}}} \tag{10}$$

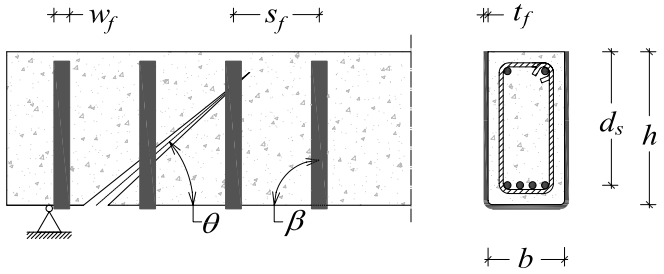

Fig. 12. Data for the externally bonded shear strengthening technique.

and f_{fdd} is the design debonding strength given as

$$f_{fdd} = \frac{0.80}{\gamma_{f,d}} \cdot \sqrt{\frac{2 \cdot E_f \cdot G_{fk}}{t_f}} \quad (11)$$

In the previous equations, h_w is the beam web depth (=h in the tested beams of the present work), f_{ctm} is the concrete average tensile strength, obtained from the average compressive strength, f_{cm}, according to CEB-FIP Model Code recommendations [20], $\gamma_{f,d}$ is a partial safety factor depending on the application accuracy, taken equal to 1.2, and G_{fk} is the specific rupture energy of the concrete-FRP bonded joint evaluated as

$$G_{fk} = 0.03 \cdot k_b \cdot \sqrt{(f_{ck} \cdot f_{ctm})} \quad (12)$$

where f_{ck} is the characteristic value of the concrete compressive strength, and k_b is a covering/scale coefficient defined as

$$k_b = \sqrt{\frac{2 - w_f/s_f}{1 + w_f/400}} \geqslant 1 \quad (13)$$

The length and force units of the variables in Eqs. (8)–(13) are millimeter and Newton, respectively. A critical shear crack angle used in the analytical formulation, $\theta^{exp.}$, was determined for each tested beam according to the major shear crack angle measured after the failure of the beam. In Table 13, the values obtained with this formulation are compared to those registered experimentally, and a F factor corresponding to the V_f^{exp}/V_{fd}^{ana} ratio is evaluated. Fig. 13 compares the values of the CRFP contribution for different critical shear crack angles according to CNR analytical model. In general, the contributions of the CFRP strengthening system predicted with this model are below the values obtained by experimental testing for all considered critical shear crack angles, with the exception of A10_M beam when $\theta = 40°$ and $\theta = 35°$, where the estimated values were slightly larger than the experimental ones (there is the suspicious that the strip crossing the shear failure crack was deficiently bonded [22]). The performance of the CNR, ACI and *fib* formulations is appraised in Fig. 14. When the value of θ is taken equal to the default value of 45° or equal to $\theta^{exp.}$, the analytical results obtained from CNR formulation are always smaller than those experimentally recorded, and the F factor follows a trend close to 1.5, as represented in Fig. 15. From the analysis of Figs. 14 and 15 it can be concluded that CNR analytical model shows a better performance for the prediction of the CFRP shear strengthening contribution rather than ACI and *fib* models. This is due to an overestimation of the effective strain derived from the ACI and *fib* formulations, as Fig. 16 shows.

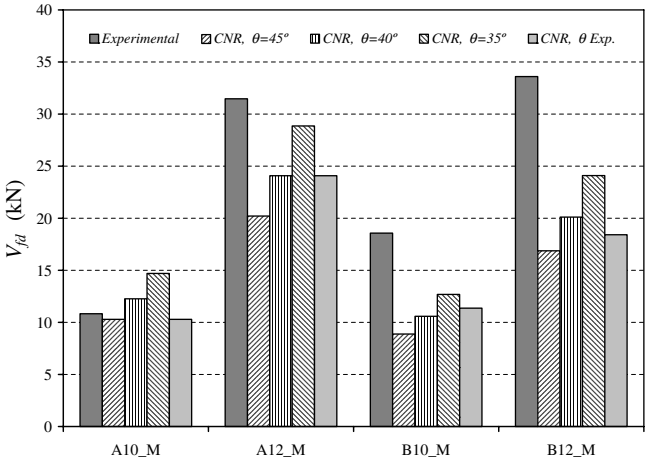

Fig. 13. Appraisal of the CNR analytical model for CFRP shear contribution.

In a previous work [22], the performance of the formulation by De Lorenzis [24] for the NSM shear strengthening of RC beams was appraised, and it was concluded that more experimental and numerical research needs to be done to develop a more confident analytical formulation, which is out of the scope of the present work.

Table 13
Analytical *vs* experimental results (CNR, ACI and *fib* analytical formulations)

Beam designation	Experimental		CNR formulation								ACI formulation		*fib* formulation	
	θ (°)	$V_f^{exp.}$ (kN)	$\theta = 45°$		$\theta = 40°$		$\theta = 35°$		θ exp		V_{fd}^{ana} (kN)	F^a	V_{fd}^{ana} (kN)	F^a
			V_{fd}^{ana} (kN)	F^a	V_{fd}^{ana} (kN)	F^a	V_{fd}^{ana} (kN)	F^a	V_{fd}^{ana} (kN)	F^a				
A10_M	45	10.8	10.3	1.05	12.3	0.88	14.7	0.74	10.3	1.05	17.0	0.64	24.0	0.45
A12_M	40	31.5	20.2	1.56	24.1	1.31	28.9	1.09	24.1	1.31	33.8	0.93	38.9	0.81
B10_M	38	18.6	8.9	2.09	10.6	1.75	12.7	1.46	11.4	1.63	17.7	1.05	20.5	0.91
B12_M	42.5	33.7	16.9	1.99	20.1	1.67	24.1	1.39	18.4	1.82	35.0	0.96	30.9	1.09

[a] $F = V_f^{exp}/V_{fd}^{ana}$.

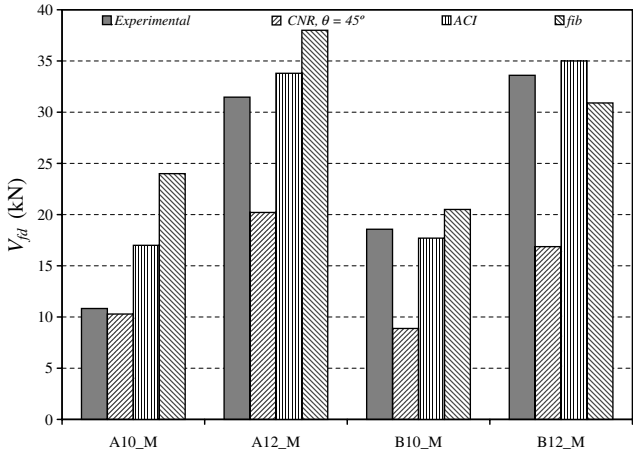

Fig. 14. Analytical and experimental results (CNR, ACI and *fib* formulations).

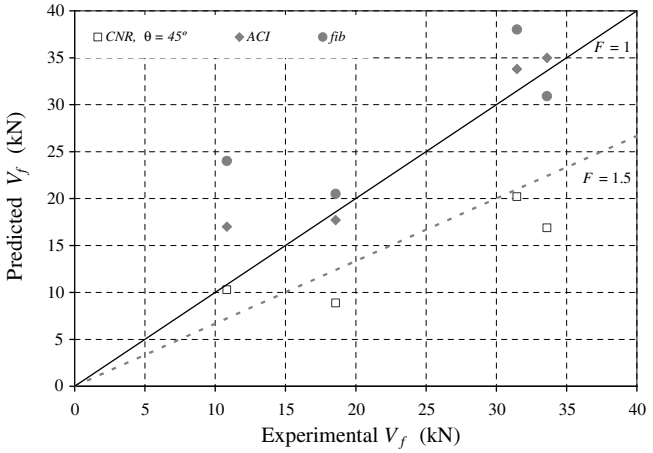

Fig. 15. Predicted *vs* experimental results (trend of *F* factors).

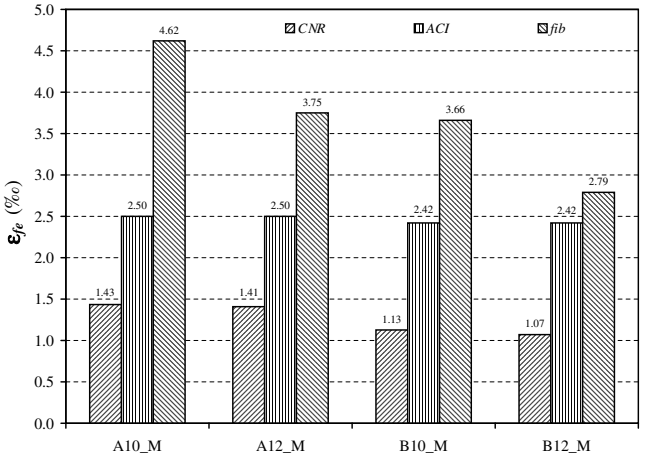

Fig. 16. Effective strain in shear reinforcement (CNR, ACI and *fib* formulations).

6. Conclusions

The effectiveness of the near surface mounted (NSM) and externally bonded reinforcing (EBR) techniques for the flexural and shear strengthening of reinforced concrete (RC) beams was compared. For this purpose, two groups of four point bending experimental tests were carried out, one for the flexural and the other for the shear strengthening, using carbon fiber reinforced polymer (CFRP) materials according to NSM and EBR techniques. For the flexural strengthening, the NSM technique was the most effective, but the difference between the efficacy of NSM and EBR techniques decreased with the increase of the longitudinal equivalent reinforcement ratio, $\rho_{l,eq}$, (steel and CFRP converted into equivalent steel). The performance of the ACI and *fib* formulations for the EBR flexural strengthening was appraised. In general, unsafe contributions of the CFRP systems were predicted, especially ACI approach for the EBR technique using wet lay-up sheets. This is caused by an overestimation of the CFRP effective strain (ε_{fe}), as a numerical model has also demonstrated, indicating that a new approach is needed to evaluate this concept. Since ACI and *fib* have not yet a dedicated formulation for the NSM technique, the carried out bending tests and the data collected from other NSM flexural strengthening experimental programs were used to show that the CFRP effective strain tends to decrease with the increase of $\rho_{l,eq}$ and with the decrease of the spacing between consecutive laminates. A numerical strategy was also used to demonstrate the decrease tendency of ε_{fe} with the increase of $\rho_{l,eq}$ in the NSM technique.

For the shear strengthening, the NSM was the most effective of the CFRP systems and was also the easiest and the fastest to apply. This efficacy was not only in terms of the beam load carrying capacity, but also in terms of deformation capacity at beam failure. Failure modes of the beams strengthened by the NSM technique were not as brittle as the ones observed in the beams strengthened by the EBR technique. The performance of the Italian design guideline (CNR) was appraised using the experimental results and the values estimated by ACI and *fib* formulations. CNR approach provided safer values than ACI and *fib* formulations.

Acknowledgements

The authors of the present work wish to acknowledge the materials provided by the S&P®, degussa® Portugal, and Secil (Unibetão, Braga). The study reported in this paper forms a part of the research program "CUTINSHEAR – Performance assessment of an innovative structural FRP strengthening technique using an integrated system based on optical fiber sensors" supported by FCT, POCTI/ECM/59033/2004. The third author acknowledges the support provided by the grant in the ambit of this research project.

References

[1] De Lorenzis L, Nanni A. Bond between near surface mounted FRP rods and concrete in structural strengthening. ACI Struct J 2002;99(2):123–33.

[2] Blaschko M, Zilch K. Rehabilitation of concrete structures with CFRP strips glued into slits. In: Proceedings of the twelfth international conference of composite materials, ICCM 12, Paris, France, 1999.
[3] Barros JAO, Fortes AS. Flexural strengthening of concrete beams with CFRP laminates bonded into slits. J Cem Concr Compos 2005;27(4):471–80.
[4] Carolin A. Carbon fibre reinforced polymers for strengthening of structural elements. PhD thesis, Lulea University of Technology, 2003.
[5] El-Hacha R, Rizkalla SH. Near-surface-mounted fiber-reinforced polymer reinforcements for flexural strengthening of concrete structures. ACI Struct J 2004;101(5):717–26.
[6] Tan K, Tumialan G, Nanni A. Evaluation of CFRP systems for the strengthening of RC slabs. CIES 02 38, Final Report, University of Missouri Rolla, 2002. 120 pp.
[7] Bonaldo E, Barros JAO. Lourenço PB. Steel fibre reinforced and laminate strips for high effective flexural strengthening of RC slabs. Report 05-DEC/E-14, Civil Engineering Department, University of Minho, Portugal, 2005. <http://www.civil.uminho.pt/composites/Publications/TR2005_001_05-DEC-E-14.pdf>.
[8] Barros JAO, Dias SJE. Shear strengthening of reinforced concrete beams with laminate strips of CFRP. International conference composites in constructions – CCC2003, Cosenza, Italy, 16–19 September 2003. p. 289–94.
[9] Nanni A, Di Ludovico M, Parretti R. Shear strengthening of a PC bridge girder with NSM CFRP rectangular bars. Adv Struct Eng 2004;7(4):97–109.
[10] ACI Committee 440. Guide for the design and construction of externally bonded FRP systems for strengthening concrete structures. American Concrete Institute; 2002. 118 pp.
[11] Fib – Bulletin 14. Externally bonded FRP reinforcement for RC structures. Technical report by Task Group 9.3 FRP (fiber reinforced polymer) reinforcement for concrete structures. Féderation Internationale du Béton – fib, July 2001. 130 pp.
[12] CNR-DT 200. Instructions for design, execution and control of strengthening interventions by means of fibre-reinforced composites. Consiglio Nazionale delle Richerche, Roma, Italy, 2004.
[13] EN 10 002-1. Metallic materials. Tensile testing. Part 1: method of test (at ambient temperature), 1990. 35 pp.
[14] ISO 527-5. Plastics – determination of tensile properties – Part 5: test conditions for unidirectional fibre-reinforced plastic composites. International Organization for Standardization, Genève, Switzerland, 1997. 9 pp.
[15] Kang J-Y, Park Y-H, Park J-S, You, Y-J, Jung, W-T. Analytical evaluation of RC beams strengthened with near surface mounted CFRP laminates. In: Proceedings of the FRP7RCS – 7th international symposium on fiber reinforced polymer reinforcement for reinforced concrete structures, Kansas City, USA, 6–9 November 2005. p. 779–94.
[16] Fortes AS. Estruturas de concreto submetidas à flexão reforçadas com laminados de CFRP colados em entalhes (NSM for the flexural strengthening of RC structures). PhD thesis, Universidade Federal de Santa Catarina, Brasil, May 2004. 213 pp [in Portuguese].
[17] Ferreira FTS, Barros JAO. Vigas de betão armado reforçadas com compósitos sujeitas a fadiga (Fatigue behavior of NSM strengthened RC beams failing in bending). Report 06-DEC/E-10, Civil Engineering Department, University of Minho, Portugal, 2006 [in Portuguese].
[18] Bonaldo E, Barros JAO, Lourenço PB. Carbon fibre laminates and fibre reinforced concrete materials for effective strengthening of RC slabs. Report 06-DEC/E-5, Civil Engineering Department, University of Minho, Portugal, 2006.
[19] Barros JAO, Oliveira JT, Lourenço PJB, Bonaldo E. Flexural behavior of reinforced masonry panels. ACI Struct J 2006;13(3):418–26.
[20] CEB-FIP Model Code. Comite Euro-International du Beton. Bulletin d'Information n° 213/214, 1993.
[21] Barros JAO, Sena-Cruz JM. Fracture energy of steel fibre reinforced concrete. J Mech Compos Mater Struct 2001;8(1):29–45.
[22] Dias SJE, Barros JAO. Shear strengthening of rectangular section RC beams with near-surface-mounted CFRP laminates. In: Proceedings of the FRP7RCS – 7th international symposium on fiber reinforced polymer reinforcement for reinforced concrete structures, Kansas City, USA, 6–9 November 2005. p. 807–24.
[23] Monti G, Liotta MA. FRP-strengthening in shear: tests and design equations. 7th International symposium on fiber reinforced polymer (FRP) reinforcement for concrete structures (FRP7RCS), Kansas, USA, 6–9 November 2005. p. 543–62.
[24] De Lorenzis L. Strengthening of RC structures with near-surface mounted FRP rods. PhD thesis in Civil Engineering, Universita' Degli Studi di Lecce, Italy, May 2002. 289 pp.
[25] ACI Committee 318. Building code requirements for structural concrete and commentary. American Concrete Institute, Reported by ACI Committee 118, 2002.